Correlated Insulators, Density Wave States, and Their Nonlinear Optical Response in Magic-Angle Twisted Bilayer Graphene

Shihao Zhang,[1] Xin Lu,[1,2] and Jianpeng Liu[1,3,*]
[1]School of Physical Science and Technology, ShanghaiTech University, Shanghai 201210, China
[2]Laboratoire de Physique des Solides, Université Paris-Sud, Université Paris Saclay, CNRS, UMR 8502, F-91405 Orsay Cedex, France
[3]ShanghaiTech Laboratory for Topological Physics, ShanghaiTech University, Shanghai 201210, China

(Received 11 October 2021; revised 26 March 2022; accepted 24 May 2022; published 17 June 2022)

The correlated insulator (CI) states and the recently discovered density wave (DW) states in magic-angle twisted bilayer graphene (TBG) have stimulated intense research interest. However, to date, the nature of these "featureless" correlated states with zero Chern numbers are still elusive and lack a characteristic experimental signature. Thus, an experimental probe to identify the characters of these featureless CI and DW states is urgently needed. In this Letter, we theoretically study the correlated insulators and density wave states at different integer and fractional fillings of the flat bands in magic-angle TBG based on extended unrestricted Hartree-Fock calculations including the Coulomb screening effects from the remote bands. We further investigate the nonlinear optical response of the various correlated states and find that the nonlinear optical conductivities can be used to identify the nature of these CI and DW states at most of the fillings. Therefore, we propose that a nonlinear optical response can serve as a promising experimental probe for unveiling the nature of the CI and DW states observed in magic-angle TBG.

DOI: 10.1103/PhysRevLett.128.247402

A twisted bilayer graphene (TBG) system around the magic angle provides a promising platform to achieve various intriguing quantum phases [1,2] such as the correlated insulators [3–12], orbital magnetic and Chern-insulator states [9,13–19], as well as unconventional superconductivity [4,10–12,20–23]. Near the magic angle 1.05° [24], there are two low-energy flat bands per spin per valley which are associated with nontrivial topological properties [25–29]. As a result, the electron-electron Coulomb interactions prevail kinetic energy, and the interplay between the strong Coulomb correlations and the nontrivial band topology give rise to diverse correlated and topological states in this system [30–49].

Most previous works focus on the integer fillings, and only a few pioneering works have paid attention to the fractional fillings of the flat bands in TBG [18,50–54], which may realize unconventional density wave (DW) states [18,50,51] and even fractional Chern-insulator states [51]. However, to date, the nature of most of the "featureless" correlated insulator (CI) states observed at integer fillings such as the zero-Chern-number CIs at $\nu = 3, 0, \pm 2$ [3,4], and the recently observed DW states at the fractional fillings $\nu = 7/2$, and $11/3$ [51], are still elusive. An experimental probe to distinguish the characters of these states is needed.

In this Letter, we use an extended unrestricted Hartree-Fock (HF) method within the subspace of the flat bands to study CIs and DW states at all integer fillings $-3 \leq \nu \leq 3$, and a few fractional fillings $\nu = 8/3$, $7/2$, and $11/3$, at which CI and DW states are observed. The Coulomb potentials acting on the flat-band subspace from the occupied remote bands are taken into account [42], and the screening of Coulomb interactions in the flat-band subspace are treated by constrained random phase approximation (CRPA). We further study different components of the nonlinear optical conductivities of all the symmetry-breaking states in the valley-sublattice space, and propose that the various competing correlated states in TBG can be identified through the nonlinear optical response.

First, we introduce the noninteracting Hamiltonian and the moiré superlattice geometries used in this Letter. In Fig. 1(a), the primitive moiré cell is marked by the black rhombus, and the real-space moiré lattice vectors of the primitive cell, the doubled supercell, and the $\sqrt{3} \times \sqrt{3}$ tripled supercell are marked by black, red, and blue vectors, respectively; the corresponding reciprocal lattice vectors and moiré Brillouin zones of the three types of moiré supercells are shown in Fig. 1(b). The low-energy effective Hamiltonian for TBG of valley μ ($\mu = \mp$ for K/K' valley) is described by the Bistritzer-MacDonald continuum model [24]

$$H_\mu^0 = \begin{pmatrix} -\hbar v_F(\mathbf{k} - \mathbf{K}_1^\mu) \cdot \boldsymbol{\sigma}_\mu & U_\mu(\mathbf{r}) \\ U_\mu^\dagger(\mathbf{r}) & -\hbar v_F(\mathbf{k} - \mathbf{K}_2^\mu) \cdot \boldsymbol{\sigma}_\mu \end{pmatrix}, \quad (1)$$

where v_F denotes the Fermi velocity, and the Hamiltonian is expanded near the Dirac points of the two layers $\mathbf{K}_1^\mu$ or

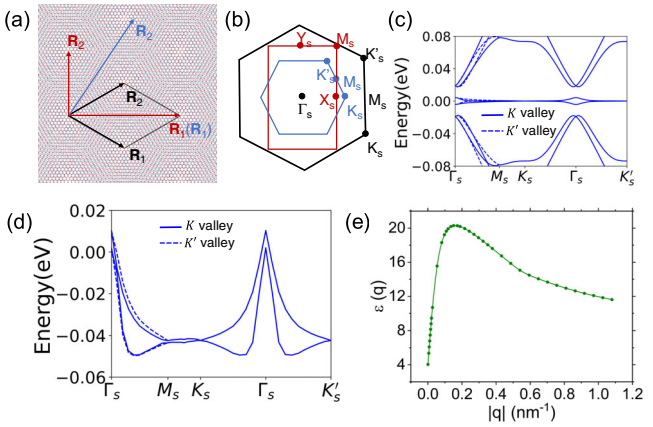

FIG. 1. (a) Illustration of the moiré superlattice of twisted bilayer graphene. The lattice vectors of the primitive moiré cell, the doubled moiré supercell, and $\sqrt{3}\times\sqrt{3}$ moiré supercell are marked by black, red, and blue arrows, respectively. (b) Moiré Brillouin zones of the primitive cell, doubled supercell, and $\sqrt{3}\times\sqrt{3}$ tripled supercell. (c) The noninteracting energy bands of magic-angle TBG, and (d) the flat-band dispersions including remote-band Hartree-Fock potentials. (e) The wave vector dependence of the effective dielectric constant calculated by CRPA method.

$\mathbf{K}_2^{\mu}$, with $\boldsymbol{\sigma}_{\mu}=(\mu\sigma_x,\sigma_y,\sigma_z)$ $(\mu=\pm)$ denoting Pauli matrices in the sublattice space. $U_{\mu}(\mathbf{r})$ refers to the interlayer coupling matrix [55]. In Fig. 1(c), we show the energy bands of the continuum model of the K valley at the magic angle $\theta=1.05°$ in the moiré Brillouin zone of the primitive cell, which can be classified into two flat bands near the charge neutrality point (CNP) and remote bands above and below them.

Now, we consider the dominant intravalley component of the long-range Coulomb interactions in the TBG system [55],

$$H_C=\frac{1}{2N_s}\sum_{\lambda\lambda'}\sum_{\mathbf{k}\mathbf{k}'\mathbf{q}}V(\mathbf{q})\hat{c}^{\dagger}_{\mathbf{k}+\mathbf{q},\lambda}\hat{c}^{\dagger}_{\mathbf{k}'-\mathbf{q},\lambda'}\hat{c}_{\mathbf{k}',\lambda'}\hat{c}_{\mathbf{k},\lambda},\quad(2)$$

where N_s denotes the total number of moiré cells in the system, $\mathbf{k}$ and $\mathbf{q}$ represent wave vectors relative to the Dirac points, $\lambda\equiv(\mu,\alpha,\sigma)$ is a composite index, with μ, α, and σ refer to the valley, layer-sublattice, and spin indices, respectively. A double-gate screened Coulomb interaction, $V(\mathbf{q})=e^2\tanh(|\mathbf{q}|d_s)/(2\Omega_M\epsilon_{\mathrm{BN}}\varepsilon_0|\mathbf{q}|)$ is adopted, where Ω_M is the area of moiré supercell, $d_s=40$ nm, $\epsilon_{\mathrm{BN}}\approx 4$ is the dielectric constant for the Boron Nitride (BN) substrate, and ε_0 is the vacuum permittivity. Then, we self-consistently solve the interacting Hamiltonian H_0+H_C with unrestricted Hartree-Fock approximation, which will be extended to be adapted for the doubled and tripled moiré supercells.

In Ref. [42] and Ref. [70], the authors propose to "regularize" the Coulomb interaction by subtracting a constant density $(1/2)\delta_{\mathbf{q},\mathbf{0}}$ from the density operator $\hat{\rho}(\mathbf{q})$, which reads

$$H'_C=\frac{N_s}{2}\sum_{\mathbf{q}}V(\mathbf{q})\delta\hat{\rho}(\mathbf{q})\delta\hat{\rho}(-\mathbf{q}),\quad(3)$$

in which $\delta\hat{\rho}(\mathbf{q})$ is defined as the density matrix at wave vector $\mathbf{q}$ subtracted by a constant $(1/2)\delta_{\mathbf{q},\mathbf{0}}$ [55]. Note that Eq. (3) is not normal ordered. After being projected onto a subset of low-energy bands, e.g., the flat bands, Eq. (3) would differ from its normal ordered form H_C, and the difference $\Delta H_C=H'_C-H_C$ can be reexpressed as the HF potentials exerted by the remote bands on the flat bands by virtue of the particle-hole and $C_{2z}\mathcal{T}$ symmetries of the projected interaction Hamiltonian [42]. In Fig. 1(d), we present the flat band structures including remote-band HF potentials. Clearly, ΔH_C significantly enhances the overall bandwidth of flat bands and induces the particle-hole asymmetry. In addition to the screening effects from the metallic gates, the Coulomb interactions between electrons in the flat bands of TBG can be further screened by virtual particle-hole excitations from the remote bands, which are treated by CRPA [71], and the details are presented in the Supplemental Material [55]. The calculated effective dielectric constant as a function of wave vector $\mathbf{q}=\tilde{\mathbf{q}}+\mathbf{Q}$ is shown in Fig. 1(e), which is consistent with the previous report [71].

We perform unrestricted HF calculations within the low-energy subspace of the flat bands including remote-band HF potentials, with the CRPA screened Coulomb interactions. First, we study the ground states at integer fillings $-3\le\nu\le 3$ without breaking moiré translational symmetry. With a realistic parameter choice of the continuum model [55,72], our calculations reveal that the ground state at the CNP is a Kramers intervalley coherent (K-IVC) state characterized by order parameters $(\tau_x,\tau_y)\sigma_y$ [34], with a mixture of small valley polarization components $|\langle\tau_z\rangle|\approx 0.1$, where $\boldsymbol{\tau}$ and $\boldsymbol{\sigma}$ denote Pauli matrices defined in the valley and sublattice space, respectively. The slight mixture of valley polarization into the K-IVC state at the CNP results from the remote-band screening effects [55]. At $\nu=\pm 1$, the HF ground state is also a mixed state with both K-IVC and spin-valley polarized (SVP) orders with Chern number ± 1, consistent with previous theoretical and experimental reports [14,35,43]. At $\nu=\pm 2$, with realistic parameter choice, we find that the ground state is a fully SVP state based on Hartree-Fock+CRPA calculations. However, if we take a fixed dielectric constant $\epsilon=10$, then, the ground state at $\nu=2$ involves the nearly degenerate IVC and SVP states [55]. This indicates that the actual ground state at $\nu=2$ is subtle and can be sensitive to details of the system. At $\nu=\pm 3$, the calculated HF ground state is always a SVP state with Chern number ± 1. In Table I, we present the dominant order parameters, symmetries, valley polarizations, Chern numbers, and gaps of the HF ground states preserving moiré translational symmetry at all integer fillings. We find that most of these CI states exhibit significant valley polarizations, which will contribute to

TABLE I. Symmetries, order parameters, valley polarizations, Chern numbers C, and gaps for the ground states at integer fillings.

ν	Order parameters	Symmetry	$\lvert\langle\tau_z\rangle\rvert$	$\lvert C\rvert$	Gap (meV)
3	$\tau_z, s_z, \tau_z s_z$	C_{3z}, C_{2x}	1	1	7.1
2	$\tau_z, s_z, \tau_z s_z$	$C_{3z}, C_{2z}\mathcal{T}, C_{2x}$	2	0	15.3
1	$(\tau_x, \tau_y)\sigma_y, \tau_z, s_z, \tau_z s_z$	C_{3z}	0.85	1	7.5
0	$(\tau_x, \tau_y)\sigma_y, \tau_z$	C_{3z}	0.10	0	25.0
−1	$(\tau_x, \tau_y)\sigma_y, \tau_z, s_z, \tau_z s_z$	C_{3z}	1.14	1	6.1
−2	$\tau_z, s_z, \tau_z s_z$	$C_{3z}, C_{2z}\mathcal{T}, C_{2x}$	2	0	14.1
−3	$\tau_z, s_z, \tau_z s_z$	C_{3z}, C_{2x}	1	1	4.4

nonlinear optical responses as will be discussed below. The band structures from the HF + CRPA calculations are given in the Supplemental Material [55].

A CI state with zero Chern number has been observed at $\nu = 3$ in TBG [4], which is inconsistent with previous theoretical results assuming preserved moiré translational symmetry [36,37,43]. Thus, one naturally expects that the zero Chern number state at $\nu = 3$ may involve a spontaneous moiré translational symmetry breaking. Therefore, in this Letter, we also perform HF calculations at $\nu = 3$ based on a doubled moiré supercell [see Figs. 1(a) and 1(b)]. Moreover, motivated by the recent discoveries of correlated states at fractional fillings of the flat bands [51], we also study the possible DW states at $\nu = 1, 7/2, 8/3$, and $11/3$. First, let us consider the DW state at $\nu = 3$ in TBG with a doubled moiré supercell. The system still stays in the SVP phase at $\nu = 3$, but there is one pair of unoccupied energy bands from the same valley-spin flavor due to the cell doubling, and both of them have zero Chern numbers. The real-space charge density distribution of this zero-Chern-number DW state is inhomogeneous around the neighboring AA sites, clearly breaks the primitive moiré translational symmetry as shown in Fig. 2(f). We also study the possible DW state with a doubled moiré supercell at $\nu = 1$, and the ground state is a SVP state with zero Chern number, with C_3-broken charge distributions as shown in Fig. 2(e). The HF band structures of these DW states with doubled primitive cells are presented in Figs. 2(a) ($\nu = 1$) and 2(b) ($\nu = 3$), where the solid blue and red dashed lines denote bands from the K and K' valleys, respectively.

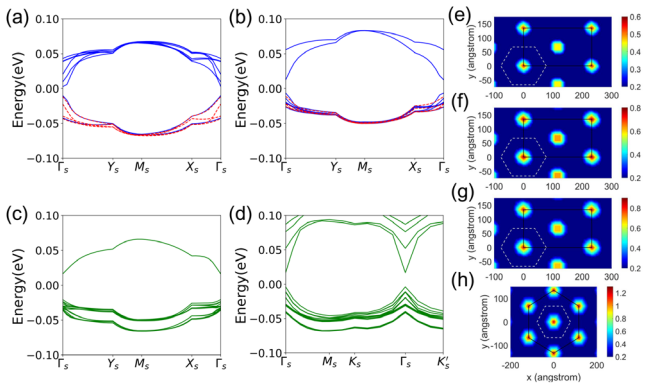

FIG. 2. The Hartree-Fock energy bands of density wave states for (a) $\nu = 1$, (b) $\nu = 3$, (c) $\nu = 7/2$, and (d) $\nu = 8/3$. The real-space distributions of charge density for (e) $\nu = 1$, (f) $\nu = 3$, (g) $\nu = 7/2$, and (h) $\nu = 8/3$. The moiré primitive cell is marked with white dashed lines.

We continue to study the DW states at fractional fillings $7/2$, $8/3$, and $11/3$, which are calculated based on doubled ($\nu = 7/2$) and $\sqrt{3} \times \sqrt{3}$ tripled ($\nu = 8/3, 11/3$) moiré supercells, respectively. The choice of such supercells can be justified by generalized susceptibility calculations [55]. The calculated ground states at $7/2$, $8/3$, and $11/3$ fillings are gapped, which may explain the experimentally observed $C = 0$ correlated insulators at $7/2$ and $11/3$ fillings, and the unusual $C = 1$ Chern insulator at $\nu = 8/3$, as reported in Ref. [51]. In particular, at $7/2$ filling, we find two nearly degenerate ground states with the energy difference $\sim 10\ \mu$eV: one is a zero-Chern-number spin-polarized K-IVC state with slight valley polarization, and the other is a SVP state having Chern number 1. We propose that the experimentally observed $C = 0$ insulator state at $7/2$ is the spin polarized K-IVC state. With doubled primitive moiré cells, there are eight flat bands from each valley, and the K-IVC order would mix the two valleys, opening a gap between the eight valence flat bands and the eight conduction flat bands, all with zero Chern numbers. At $7/2$ filling, seven out of the eight conduction flat bands are filled, yielding a zero-Chern-number spin polarized K-IVC state. The single-particle spectrum around $7/2$ filling is presented in Fig. 2(c).

At $8/3$ filling, based on $\sqrt{3} \times \sqrt{3}$ tripled supercell HF calculations, we find the ground state is a SVP state with a slight mixture of K-IVC order, and the calculated Chern number of this state is 1 [55], consistent with experiments [51]. Such a state is adiabatically connected to a pure SVP state with Chern number 1 [55]. At $11/3$ filling, the ground state turns out to be a pure SVP state with zero Chern number. It should be noted that the bandwidth of the conduction flat band can be significantly reduced in the presence of vertical magnetic fields due to the orbital magnetic effects concomitant with a more uniform

TABLE II. Symmetries, order parameters, valley polarizations $\langle\tau_z\rangle$, K-IVC order amplitudes and gaps for the different DW states.

ν	Main order parameters	Symmetry	$\lvert\langle\tau_z\rangle\rvert$	IVC	Gap (meV)
1	$\tau_z, s_z, \tau_z s_z$	$C_{2z}\mathcal{T}$	6	0	12.7
3	$\tau_z, s_z, \tau_z s_z$	$C_{2z}\mathcal{T}$	2	0	17.2
7/2	$(\tau_x, \tau_y)\sigma_y s_{0,z}, s_z$	$\mathcal{T}'$	0.07	0.45	35.7
8/3	$\tau_z, s_z, \tau_z s_z, (\tau_x, \tau_y)\sigma_y$	C_{3z}	3.65	0.54	20.6
11/3	$\tau_z, s_z, \tau_z s_z$	$C_{2z}\mathcal{T}, C_{3z}$	1	0	52.4

distribution of Berry curvatures [51,73]. As a result, around filling 11/3, the system would undergo a transition from the DW state to the fractional Chern insulator state with increased magnetic field [51,73].

The Hartree-Fock band structures at 7/2 and 8/3 fillings are presented in Figs. 2(c) and 2(d), respectively. The corresponding ground-state real-space charge density distributions are presented in Fig. 2(g) ($\nu = 7/2$) and (h) ($\nu = 8/3$), respectively. The leading order parameters, symmetries, the calculated valley polarizations $\langle\tau_z\rangle$, and the calculated IVC order amplitudes in the different DW states at $\nu = 1, 3, 7/2, 8/3$, and 11/3 are presented in Table. II.

Quite a few of the experimentally observed CIs and DWs in magic-angle TBG are featureless insulators, such as the CIs observed at the CNP, $\nu = \pm 2$, the CI at $\nu = 3$, and the DW states at 7/2, etc. All of these states are just insulating with zero Chern number, and do not exhibit any particular signature in conventional transport and optical approaches. Therefore, it is difficult to experimentally identify the nature of these correlated states. Here, we propose that these featureless correlated states may exhibit distinct nonlinear optical responses, which is described by the generation of an alternating current density $j^c(\omega_1 + \omega_2)$ due to the second-order response to the electric fields

$$j^c(\omega_1 + \omega_2) = \sum_{a,b=x,y} \sigma^c_{ab}(\omega_1 + \omega_2) E_a(\omega_1) E_b(\omega_2). \quad (4)$$

The nonlinear optical conductivity tensor σ^c_{ab} may serve as a promising probe to unveil the nature of the various correlated states observed in magic-angle TBG. In this Letter, we study two kinds of nonlinear optical processes, the shift-current response with $\omega_1 = -\omega_2 = \omega$, and the second harmonic generation (SHG) with $\omega_1 = \omega_2 = \omega$. For SHG response, the nonlinear susceptibility $\chi^c_{ab}(2\omega) = i\sigma^c_{ab}(2\omega)/(\varepsilon_0 2\omega)$.

We illustrate our idea by comparing the nonlinear optical responses of two prototypical CIs, both with zero Chern numbers: a K-IVC state characterized by order parameter $(\tau_x\sigma_y, \tau_y\sigma_y)$, and a valley-polarized (VP) state characterized by order parameter τ_z. A VP order actually spontaneously breaks both C_{2z}, time-reversal ($\mathcal{T}$), and C_{2y} symmetries and preserves $C_{2z}\mathcal{T}$, C_{3z}, and C_{2x} symmetries. Such a state exhibits counter-propagating current loops in real space, which contribute to staggered orbital magnetic fluxes [35]. Since both C_{2z} and $\mathcal{T}$ symmetries are broken due to such a real-space current pattern (although $C_{2z}\mathcal{T}$ is preserved), a VP state can have a nonlinear optical response with symmetry-allowed nonlinear optical conductivity components: $\sigma^x_{xx}(\omega) = -\sigma^y_{xy}(\omega) = -\sigma^y_{yx}(\omega) = -\sigma^x_{yy}(\omega)$ [55]. In particular, a nonvanishing $\sigma^x_{xx}(\omega)$ component is a smoking gun for the valley polarization, i.e., $\sigma^x_{xx}(\omega) = \sigma^x_{xx,z}(\omega)\langle\tau_z\rangle$ [55]. On the other hand, although a K-IVC order $(\tau_x\sigma_y, \tau_y\sigma_y)$ generally breaks C_{2z} symmetry, the combination of C_{2z} symmetry and a $C'_{2z} = \tau_z C_{2z}$ symmetry, would enforce the vanishing nonlinear optical response of a K-IVC state [55]. Thus, nonlinear optics can be considered as a reliable approach to distinguish the VP and K-IVC states. Further analysis reveals that all the IVC states have a vanishing nonlinear optical response, and there are only three types of order parameters, i.e., the VP order τ_z, the "nematic order" $(\tau_z\sigma_x, \sigma_y)$, and the sublattice order σ_z, that are allowed to have nonzero nonlinear optical responses in TBG [55]. We note that the order parameters $(\tau_z\sigma_x, \sigma_y)$ are also involved in the "incommensurate Kekulé state" which is proposed as the ground state at nonzero fillings of magic-angle TBG under finite strain [53].

In order to verify the above argument, we have numerically calculated the SHG susceptibility and nonlinear photo conductivity for the shift current for various different ordered states in TBG, assuming a constant, **k** independent order parameter with amplitude of 1 meV in each state, with the filling fixed at the CNP. The results are presented in Fig. 3(a) (for SHG) and 3(b) (for shift current). We see that

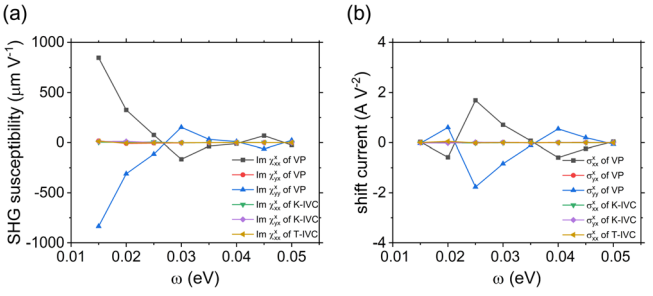

FIG. 3. The nonlinear optical response of TBG at the CNP assuming constant order parameters with amplitudes (1 meV) applied to the flat bands.

the nonlinear susceptibilities vanish for both the K-IVC state, and the time-reversal invariant intervalley coherent (T-IVC) state characterized by order parameter $(\tau_x\sigma_x, \tau_y\sigma_x)$. In contrast, the SHG susceptibility and shift-current conductivity of a VP state are giant in the infrared frequency regime $\hbar\omega \sim 15$–25 meV.

Now, we discuss the feasibility of performing nonlinear optical measurements for a magic-angle TBG device. Nowadays, the size of a good TBG sample can be made more than 10 μm in each lateral direction, whereas the spot size of a laser beam in the infrared frequency regime (say, with the wavelength of 2500 nm) can be adjusted to $\sim$5 μm [74,75], smaller than the size of the TBG sample. Thus, one can safely rule out any undesirable response from the sample boundaries, and directly perform SHG rotation anisotropy measurements for a bottom-gated TBG device with vertical incident light. Actually, SHG measurements have already been performed for a non-magic-angle TBG device [75]. By virtue of the chiral structure of TBG, a remarkable second-harmonic signal contributed by the χ_{xyz} component of the SHG susceptibility tensor has been observed [75]. This experiment indicates that performing SHG measurements on a magic-angle TBG device is promising and feasible. Moreover, given that a couple of "hidden" correlated phases have already been unveiled by SHG measurements in some strongly correlated systems such as cuprates and iridates [76–78], we would expect the successful application of this technique to the magic-angle TBG system as well.

To summarize, in this Letter, we have theoretically studied the correlated insulators and density wave states at various integer and fractional fillings of the flat bands based on extended unrestricted HF calculations with screening effects treated by CRPA method. We have explained the nature of the recently observed density wave states and symmetry-breaking Chern insulator states at $\nu = 1, 3, 7/2$, and $8/3$ fillings. We also find that most of the CI and DW states exhibit substantial valley polarizations, which would contribute to a giant nonlinear optical response. We have identified the symmetry-allowed nonlinear optical conductivity components in different types of ordered states. Our results indicate that a nonlinear optical response may serve as a promising probe to distinguish different types of correlated states observed in magic-angle TBG, which would stimulate further experimental and theoretical studies on the nonlinear optical properties of moiré 2D systems.

This work is supported by the National Key R&D program of China (Grant No. 2020YFA0309601), the National Natural Science Foundation of China (Grant No. 12174257), and the start-up grant of ShanghaiTech University. We would like to thank Professor Xi Dai and Professor Jian Kang for valuable discussions. We thank the HPC platform of ShanghaiTech University for providing the computational resource.

Note added.—Recently, a few related works have come to out attention: in Ref. [79], the authors have extensively studied the incommensurate Kekulé state at noninteger fillings of TBG; in Refs. [80,81], two theory groups independently proposed distinguishing the different correlated states in magic-angle TBG using scanning tunneling microscopy.

*liujp@shanghaitech.edu.cn

[1] L. Balents, C. R. Dean, D. K. Efetov, and A. F. Young, Nat. Phys. **16**, 725 (2020).
[2] E. Y. Andrei, D. K. Efetov, P. Jarillo-Herrero, A. H. MacDonald, K. F. Mak, T. Senthil, E. Tutuc, A. Yazdani, and A. F. Young, Nat. Rev. Mater. **6**, 201 (2021).
[3] Y. Cao, V. Fatemi, A. Demir, S. Fang, S. L. Tomarken, J. Y. Luo, J. D. Sanchez-Yamagishi, K. Watanabe, T. Taniguchi, E. Kaxiras *et al.*, Nature (London) **556**, 80 (2018).
[4] X. Lu, P. Stepanov, W. Yang, M. Xie, M. A. Aamir, I. Das, C. Urgell, K. Watanabe, T. Taniguchi, G. Zhang *et al.*, Nature (London) **574**, 653 (2019).
[5] A. Kerelsky, L. J. McGilly, D. M. Kennes, L. Xian, M. Yankowitz, S. Chen, K. Watanabe, T. Taniguchi, J. Hone, C. Dean *et al.*, Nature (London) **572**, 95 (2019).
[6] Y. Jiang, X. Lai, K. Watanabe, T. Taniguchi, K. Haule, J. Mao, and E. Y. Andrei, Nature (London) **573**, 91 (2019).
[7] Y. Xie, B. Lian, B. Jäck, X. Liu, C.-L. Chiu, K. Watanabe, T. Taniguchi, B. A. Bernevig, and A. Yazdani, Nature (London) **572**, 101 (2019).
[8] Y. Choi, J. Kemmer, Y. Peng, A. Thomson, H. Arora, R. Polski, Y. Zhang, H. Ren, J. Alicea, G. Refael *et al.*, Nat. Phys. **15**, 1174 (2019).
[9] M. Serlin, C. Tschirhart, H. Polshyn, Y. Zhang, J. Zhu, K. Watanabe, T. Taniguchi, L. Balents, and A. Young, Science **367**, 900 (2019).
[10] P. Stepanov, I. Das, X. Lu, A. Fahimniya, K. Watanabe, T. Taniguchi, F. H. L. Koppens, J. Lischner, L. Levitov, and D. K. Efetov, Nature (London) **583**, 375 (2020).
[11] Y. Saito, J. Ge, K. Watanabe, T. Taniguchi, and A. F. Young, Nat. Phys. **16**, 926 (2020).
[12] X. Liu, Z. Wang, K. Watanabe, T. Taniguchi, O. Vafek, and J. Li, Science **371**, 1261 (2021).
[13] A. L. Sharpe, E. J. Fox, A. W. Barnard, J. Finney, K. Watanabe, T. Taniguchi, M. A. Kastner, and D. Goldhaber-Gordon, Science **365**, 605 (2019).
[14] P. Stepanov, M. Xie, T. Taniguchi, K. Watanabe, X. Lu, A. H. MacDonald, B. A. Bernevig, and D. K. Efetov, Phys. Rev. Lett. **127**, 197701 (2021).
[15] K. P. Nuckolls, M. Oh, D. Wong, B. Lian, K. Watanabe, T. Taniguchi, B. A. Bernevig, and A. Yazdani, Nature (London) **588**, 610 (2020).
[16] S. Wu, Z. Zhang, K. Watanabe, T. Taniguchi, and E. Y. Andrei, Nat. Mater. **20**, 488 (2021).
[17] I. Das, X. Lu, J. Herzog-Arbeitman, Z.-D. Song, K. Watanabe, T. Taniguchi, B. A. Bernevig, and D. K. Efetov, Nat. Phys. **17**, 710 (2021).
[18] A. T. Pierce, Y. Xie, J. M. Park, E. Khalaf, S. H. Lee, Y. Cao, D. E. Parker, P. R. Forrester, S. Chen, K. Watanabe *et al.*, Nat. Phys. **17**, 1210 (2021).

[19] J. Liu and X. Dai, Nat. Rev. Phys. **3**, 367 (2021).
[20] Y. Cao, V. Fatemi, S. Fang, K. Watanabe, T. Taniguchi, E. Kaxiras, and P. Jarillo-Herrero, Nature (London) **556**, 43 (2018).
[21] M. Yankowitz, S. Chen, H. Polshyn, Y. Zhang, K. Watanabe, T. Taniguchi, D. Graf, A. F. Young, and C. R. Dean, Science **363**, 1059 (2019).
[22] E. Codecido, Q. Wang, R. Koester, S. Che, H. Tian, R. Lv, S. Tran, K. Watanabe, T. Taniguchi, F. Zhang *et al.*, Sci. Adv. **5**, eaaw9770 (2019).
[23] Y. Cao, D. Rodan-Legrain, J. M. Park, N. F. Yuan, K. Watanabe, T. Taniguchi, R. M. Fernandes, L. Fu, and P. Jarillo-Herrero, Science **372**, 264 (2021).
[24] R. Bistritzer and A. H. MacDonald, Proc. Natl. Acad. Sci. U.S.A. **108**, 12233 (2011).
[25] Z. Song, Z. Wang, W. Shi, G. Li, C. Fang, and B. A. Bernevig, Phys. Rev. Lett. **123**, 036401 (2019).
[26] J. Ahn, S. Park, and B.-J. Yang, Phys. Rev. X **9**, 021013 (2019).
[27] H. C. Po, L. Zou, T. Senthil, and A. Vishwanath, Phys. Rev. B **99**, 195455 (2019).
[28] G. Tarnopolsky, A. J. Kruchkov, and A. Vishwanath, Phys. Rev. Lett. **122**, 106405 (2019).
[29] J. Liu, J. Liu, and X. Dai, Phys. Rev. B **99**, 155415 (2019).
[30] J. Kang and O. Vafek, Phys. Rev. Lett. **122**, 246401 (2019).
[31] K. Seo, V. N. Kotov, and B. Uchoa, Phys. Rev. Lett. **122**, 246402 (2019).
[32] M. Xie and A. H. MacDonald, Phys. Rev. Lett. **124**, 097601 (2020).
[33] N. Bultinck, S. Chatterjee, and M. P. Zaletel, Phys. Rev. Lett. **124**, 166601 (2020).
[34] N. Bultinck, E. Khalaf, S. Liu, S. Chatterjee, A. Vishwanath, and M. P. Zaletel, Phys. Rev. X **10**, 031034 (2020).
[35] J. Liu and X. Dai, Phys. Rev. B **103**, 035427 (2021).
[36] Y. Zhang, K. Jiang, Z. Wang, and F. Zhang, Phys. Rev. B **102**, 035136 (2020).
[37] K. Hejazi, X. Chen, and L. Balents, Phys. Rev. Research **3**, 013242 (2021).
[38] J. Kang and O. Vafek, Phys. Rev. B **102**, 035161 (2020).
[39] B.-B. Chen, Y. D. Liao, Z. Chen, O. Vafek, J. Kang, W. Li, and Z. Y. Meng, Nat. Commun. **12**, 5480 (2021).
[40] C. Lu, Y. Zhang, Y. Zhang, M. Zhang, C.-C. Liu, Z.-C. Gu, W.-Q. Chen, and F. Yang, arXiv:2003.09513.
[41] Y. D. Liao, J. Kang, C. N. Breiø, X. Y. Xu, H.-Q. Wu, B. M. Andersen, R. M. Fernandes, and Z. Y. Meng, Phys. Rev. X **11**, 011014 (2021).
[42] B. A. Bernevig, Z.-D. Song, N. Regnault, and B. Lian, Phys. Rev. B **103**, 205413 (2021).
[43] B. Lian, Z.-D. Song, N. Regnault, D. K. Efetov, A. Yazdani, and B. A. Bernevig, Phys. Rev. B **103**, 205414 (2021).
[44] F. Xie, A. Cowsik, Z.-D. Song, B. Lian, B. A. Bernevig, and N. Regnault, Phys. Rev. B **103**, 205416 (2021).
[45] T. Soejima, D. E. Parker, N. Bultinck, J. Hauschild, and M. P. Zaletel, Phys. Rev. B **102**, 205111 (2020).
[46] P. Potasz, M. Xie, and A. H. MacDonald, Phys. Rev. Lett. **127**, 147203 (2021).
[47] X. Zhang, G. Pan, Y. Zhang, J. Kang, and Z. Y. Meng, Chin. Phys. Lett. **38**, 077305 (2021).
[48] J. S. Hofmann, E. Khalaf, A. Vishwanath, E. Berg, and J. Y. Lee, arXiv:2105.12112.
[49] D. E. Parker, T. Soejima, J. Hauschild, M. P. Zaletel, and N. Bultinck, Phys. Rev. Lett. **127**, 027601 (2021).
[50] H. Polshyn, Y. Zhang, M. A. Kumar, T. Soejima, P. Ledwith, K. Watanabe, T. Taniguchi, A. Vishwanath, M. P. Zaletel, and A. F. Young, Nat. Phys. **18**, 42 (2022).
[51] Y. Xie, A. T. Pierce, J. M. Park, D. E. Parker, E. Khalaf, P. Ledwith, Y. Cao, S. H. Lee, S. Chen, P. R. Forrester *et al.*, Nature (London) **600**, 439 (2021).
[52] B. Padhi, C. Setty, and P. W. Phillips, Nano Lett. **18**, 6175 (2018).
[53] Y. H. Kwan, G. Wagner, T. Soejima, M. P. Zaletel, S. H. Simon, S. A. Parameswaran, and N. Bultinck, Phys. Rev. X **11**, 041063 (2021).
[54] K. Zhang, Y. Zhang, L. Fu, and E.-A. Kim, arXiv:2105.13371.
[55] See Supplemental Material at http://link.aps.org/supplemental/10.1103/PhysRevLett.128.247402 for: (a) the details for the continuum model of twisted bilayer graphene, (b) the Coulomb interactions and the Hartree-Fock method, (c) screening effects from the remote bands treated by constrained random phase approximation, (d) more results about Hartree-Fock ground states and single-particle excitations at integer fillings with preserved translational symmetry, (e) analysis about the nature of the density wave states, (f) generalized susceptibility calculations, (g) symmetry analysis on the nonlinear optical response in different ordered phases and discussions on the strain effects, and (h) microscopic expressions for the nonlinear optical response, which includes Refs. [56–69].
[56] J. M. Pizarro, M. Rösner, R. Thomale, R. Valentí, and T. O. Wehling, Phys. Rev. B **100**, 161102(R) (2019).
[57] J. Rath and A. J. Freeman, Phys. Rev. B **11**, 2109 (1975).
[58] D. Wong, K. P. Nuckolls, M. Oh, B. Lian, Y. Xie, S. Jeon, K. Watanabe, T. Taniguchi, B. A. Bernevig, and A. Yazdani, Nature (London) **582**, 198 (2020).
[59] U. Zondiner, A. Rozen, D. Rodan-Legrain, Y. Cao, R. Queiroz, T. Taniguchi, K. Watanabe, Y. Oreg, F. von Oppen, A. Stern *et al.*, Nature (London) **582**, 203 (2020).
[60] S. Liu, E. Khalaf, J. Y. Lee, and A. Vishwanath, Phys. Rev. Research **3**, 013033 (2021).
[61] P. J. Ledwith, G. Tarnopolsky, E. Khalaf, and A. Vishwanath, Phys. Rev. Research **2**, 023237 (2020).
[62] P. J. Ledwith, E. Khalaf, and A. Vishwanath, Ann. Phys. (Amsterdam) **435**, 168646 (2021).
[63] K. Hejazi, C. Liu, H. Shapourian, X. Chen, and L. Balents, Phys. Rev. B **99**, 035111 (2019).
[64] S. Zhang, X. Dai, and J. Liu, Phys. Rev. Lett. **128**, 026403 (2022).
[65] R. von Baltz and W. Kraut, Phys. Rev. B **23**, 5590 (1981).
[66] Y. Zhang, H. Ishizuka, J. van den Brink, C. Felser, B. Yan, and N. Nagaosa, Phys. Rev. B **97**, 241118(R) (2018).
[67] J. Liu and X. Dai, npj Comput. Mater. **6**, 57 (2020).
[68] Y. Zhang, T. Holder, H. Ishizuka, F. de Juan, N. Nagaosa, C. Felser, and B. Yan, Nat. Commun. **10**, 1 (2019).
[69] T. Holder, D. Kaplan, and B. Yan, Phys. Rev. Research **2**, 033100 (2020).
[70] J. Kang, B. A. Bernevig, and O. Vafek, Phys. Rev. Lett. **127**, 266402 (2021).
[71] T. I. Vanhala and L. Pollet, Phys. Rev. B **102**, 035154 (2020).

[72] M. Koshino, N. F. Q. Yuan, T. Koretsune, M. Ochi, K. Kuroki, and L. Fu, Phys. Rev. X **8**, 031087 (2018).
[73] D. Parker, P. Ledwith, E. Khalaf, T. Soejima, J. Hauschild, Y. Xie, A. Pierce, M. P. Zaletel, A. Yacoby, and A. Vishwanath, arXiv:2112.13837.
[74] C. Du and J. A. McGuire (private communication).
[75] F. Yang, W. Song, F. Meng, F. Luo, S. Lou, S. Lin, Z. Gong, J. Cao, E. S. Barnard, E. Chan *et al.*, Matter Radiat. Extremes **3**, 1361 (2020).
[76] A. d. l. Torre, K. L. Seyler, L. Zhao, S. D. Matteo, M. S. Scheurer, Y. Li, B. Yu, M. Greven, S. Sachdev, M. R. Norman, and D. Hsieh, Nat. Phys. **17**, 777 (2021).
[77] L. Zhao, D. H. Torchinsky, H. Chu, V. Ivanov, R. Lifshitz, R. Flint, T. Qi, G. Cao, and D. Hsieh, Nat. Phys. **12**, 32 (2016).
[78] J. W. Harter, Z. Y. Zhao, J.-Q. Yan, D. G. Mandrus, and D. Hsieh, Science **356**, 295 (2017).
[79] G. Wagner, Y. H. Kwan, N. Bultinck, S. H. Simon, and S. A. Parameswaran, Phys. Rev. Lett. **128**, 156401 (2022).
[80] D. Călugăru, N. Regnault, M. Oh, K. P. Nuckolls, D. Wong, R. L. Lee, A. Yazdani, O. Vafek, and B. A. Bernevig, arXiv:2110.15300.
[81] J. P. Hong, T. Soejima, and M. P. Zaletel, arXiv:2110.14674.